Applied Surface Science Advances 27 (2025) 100762

Contents lists available at ScienceDirect

Applied Surface Science Advances

journal homepage: www.sciencedirect.com/journal/applied-surface-science-advances

Full Length Article

Quantum fluorescent gold nanoclusters for PCR-free ultrasensitive DNA detection

Regina Maria Chiechio [*,a], Antonino Scandurra [a,b,c], Riccardo Reitano [a], Paolo Musumeci [a], Maria Grazia Grimaldi [a,b], Annalinda Contino [d], Giuseppe Maccarrone [d], Valerie Marchi [e], Ludovica Maugeri [f], Salvatore Petralia [*,f,g], Francesco Ruffino [a,b]

[a] Dipartimento di Fisica e Astronomia "Ettore Majorana" Università di Catania, Via S. Sofia 64, 95123, Catania, Italy
[b] CNR-IMM, Via S. Sofia 64, 95123, Catania, Italy
[c] Research Unit of the University of Catania, National Inter University Consortium of Materials Science and Technology (INSTM-UdR of Catania), Via Santa Sofia 64, 95125 Catania, Italy
[d] Dipartimento di Scienze Chimiche, Università degli Studi di Catania, Catania 95125, Italy
[e] Institut des Sciences Chimiques de Rennes ISCR, UMR CNRS 6226, University Rennes, 35042 Rennes, France
[f] Department of Drug and Health Sciences, University of Catania, 95125 Catania, Italy
[g] CNR-Institute of Biomolecular Chemistry, Via Paolo Gaifami 18, 95126 Catania, Italy

ARTICLE INFO

Keywords:
Gold nanoclusters
PCR-free biosensor
DNA functionalization
Fluorescence quenching
Ultrasensitive detection
Eco-friendly synthesis

ABSTRACT

Gold nanoclusters (AuNCs) have emerged as promising tools for biomedical and environmental applications due to their photoluminescence, biocompatibility, and molecule-like electronic structure. This study presents a novel AuNC-based sensor platform, characterized by eco-friendly synthesis, label-free functionality, and ultrasensitivity for biomolecular detection. AuNCs were synthesized using a green chemistry approach without toxic solvents, yielding strong optical properties with an absorbance peak at 400 nm and emission at 600 nm. Functionalization with thiolated single-stranded DNA (ssDNA) enabled fluorescence-based detection of specific DNA sequences with a limit of detection in the attomolar range. The sensor demonstrated high specificity, distinguishing target DNA from non-specific sequences in both buffer solutions and complex biological matrices, including blood. The modular design allows adaptation to detect various biomolecules by incorporating specific aptamers. This versatile, cost-effective platform combines eco-friendly synthesis, high sensitivity, and specificity, offering significant potential for advanced diagnostics and environmental monitoring in real-world settings.

1. Introduction

In recent years, gold nanoclusters (AuNCs) have attracted great interest owing to their unique properties, including photoluminescence, biocompatibility, and rapid renal clearance, making them promising for various biomedical applications [1–4]. Unlike larger gold nanoparticles, which exhibit plasmonic effects, AuNCs, typically smaller than 2 nm, display optical properties similar to those of molecules. This unique quantum confinement gives them a discrete electronic structure, enabling fluorescence emission across a broad spectrum [5–9]. This characteristic has facilitated the use of AuNCs in bioimaging and theragnostic applications. Beyond these applications, encapsulating AuNCs in liposomes[10] or biological vesicles[11] have been previously demonstrated to deliver them in biological environments and enable targeted drug release, improving therapeutic efficacy [12,13].

Despite these advances, the development of highly sensitive, specific, and environmentally friendly sensors remains a critical challenge, especially for detecting analytes in complex biological environments. In medical diagnostics, there is an increasing need for sensors capable of detecting biomarkers at extremely low concentrations (in the femtomolar to attomolar range) to enable early diagnosis of diseases. Early detection is essential, as many biomarkers, such as those for cancer or neurodegenerative diseases, are present in trace amounts in the initial stages. Therefore, more sensitive sensors are needed to improve early diagnosis and treatment outcomes [14]. Furthermore, current sensing technologies often rely on labeling, complex surface modifications, or the use of toxic solvents, which limit their applicability and sustainability. There is a pressing need for sensors that not only achieve high

* Corresponding authors.
E-mail addresses: regina.chiechio@dfa.unict.it (R.M. Chiechio), salvatore.petralia@unict.it (S. Petralia).

https://doi.org/10.1016/j.apsadv.2025.100762
Received 26 February 2025; Received in revised form 28 April 2025; Accepted 29 April 2025
Available online 10 May 2025
2666-5239/© 2025 The Author(s). Published by Elsevier B.V. This is an open access article under the CC BY-NC-ND license (http://creativecommons.org/licenses/by-nc-nd/4.0/).

sensitivity but also offer simplicity, eco-friendliness, and applicability in real-world conditions without the drawbacks of conventional methods [15–17].

Modern biosensing technologies often achieve high sensitivity through enzymatic amplification, high-performance nanomaterials, or surface engineering strategies. For instance, techniques such as polymerase chain reaction (PCR) enable femtomolar detection of nucleic acids [18], while fluorescent biosensors based on semiconductor quantum dots leverage their high quantum yield to detect biological targets with high precision [19]. However, these approaches often suffer from significant drawbacks, including complexity, the need for labeling or amplification, limited biocompatibility, and the use of toxic or environmentally harmful materials [20,21].

Among the various approaches, several strategies based on nanomaterials for nucleic acid sensing have demonstrated remarkable analytical performance. For instance, fluorescent platforms based on graphene quantum dots or carbon nanomaterials have achieved sub-femtomolar sensitivity. More recently, electrochemical biosensors incorporating nanostructures such as gold nanoparticles, graphene oxide, and metal–organic frameworks have pushed detection limits down to the attomolar range for microRNA targets [22]. Although these methods are extremely effective, they often rely on enzymatic amplification or multi-component systems, which may introduce complexity and reduce biocompatibility. Therefore, the development of simpler, robust, and eco-friendly biosensing platforms remains an active area of research.

In this context, AuNCs hold significant potential in sensing, offering a safer and more accessible alternative to conventional approaches while achieving lower or comparable LODs. Their intrinsic fluorescence, the specific binding capabilities provided by surface ligands, and their ultrasmall size make them a versatile platform for the sensitive and specific detection of various analytes, including heavy metals, protein biomarkers, and nucleic acids, as well as for applications in complex *in vivo* systems [23,24].

AuNCs have been used to detect heavy metal ions like Hg^{2+} and Cu^{2+} through a “turn-off” mechanism based on fluorescence quenching. This mechanism enables the detection of low analyte concentrations, with detection limits (LOD) down to a few ppm for various ions [25–27].

AuNCs have also shown promise in the detection of protein biomarkers. Hosseini et al. developed a "turn-on" fluorescent sensor for the ultrasensitive detection of neuron-specific enolase (NSE), a tumor biomarker, achieving an LOD of around 2.0 pg/mL [28]. More recently, AuNCs functionalized with DNA have been developed for the detection of proteins such as mucin 1, CA125, and carcinoembryonic antigen, using graphene oxide as a quencher [29]. Additionally, You and Tseng proposed a peptide-induced aggregation strategy to enhance the emission of GSH-AuNCs, demonstrating how controlled aggregation can increase fluorescence intensity in the presence of target analytes [30]. Another relevant application area for AuNCs is nucleic acid sensing. For instance, Wang et al. developed a biosensor based on DNA-functionalized AuNCs combined with MnO_2 nanosheets, employing a fluorescence quenching and reactivation mechanism to detect specific DNA sequences, with a reported LOD of 0.1 nM [31]. In a similar approach, Borghei et al. designed functionalized AuNCs for the detection of miRNA using a photoinduced “turn-off” mechanism, achieving a LOD of 60 fM [32].

However, these methods often face significant challenges, including lack of specificity, the requirement for additional quenchers, complicated surface modifications, or insufficient low detection limits (LOD). These limitations hinder their effectiveness and practical applicability in real-world scenarios. To overcome these challenges, this study introduces a novel AuNC-based sensor entirely label-free, eco-friendly, and easy to functionalize. Our sensor is synthesized without the use of toxic organic solvents with a rapid and simple functionalization process. The possibility to functionalize it with aptamers also makes it easily adaptable for detecting a wide variety of analytes. This results in an extremely sensitive (attomolar LOD) and selective sensor that can detect analytes even in complex biological matrices, such as blood, making it highly suitable for both medical diagnostics and environmental monitoring.

2. Experimental section

2.1. Reagents and materials

Oligonucleotides were purchased by IDT (Integrated DNA Technologies) and used as received. The probe 5’-/5ThioMC6-D/GTC TCG ATA TCA TAT CGT TGA CTT TA-3’ (ssDNA-probe, MW=8254,6 g/mol), target complementary 5’-TAA AGT CAA CGA TAT GAT ATC GAG AC-3’ (ssDNA-target, MW=8190,4 g/mol) and the unspecific GGAGACCAA-TAGAAACTGGGC (MW 6514,2 ug/umol) were used for the experiments. MES buffer, Chloroauric acid ($HAuCl_4$), Glutathione (GSH), Amicon Ultra were purchased by Merck. The solutions were prepared by de-ionized water treated in a MilliQ™ system.

2.2. Sensor fabrication

2.2.1. Gold nanoclusters synthesis

AuNCs were synthesized by adding in a 100 mL flask, 33.6 mL of MilliQ™ water and 2.4 mL of aqueous solution of GSH (50 mM) immediately prepared before use; then, 4 mL of a solution of $HAuCl_4$ (20 mM) was added under stirring, and the solution was immediately moved on a hot plate set at 120°C to get a reflux. The as-obtained solution was left to stir for 3 h. An aqueous suspension of orange-emitting GSHAuNCs was formed. The NCs suspension obtained could be stored at 4°C for several months with negligible changes in their optical properties. All glassware used for these syntheses was cleaned in a bath of freshly prepared aqua regia and rinsed 10 times in water before use [33,34].

2.2.2. Purification of GSH NCs and functionalization with ss-DNA probe

The gold nanoclusters were purified from GSH excess starting from a 3 mL suspension of GSH NCs. The suspension was purified by ultrafiltration using centrifugal Amicon filter (3 kDa), and MES buffer solution (50 mM, pH 6). The centrifugation was conducted at 12,000 g for 7 minutes and repeated three times, washing with the buffer solution each time (Procedure-2: Optimized). In the case of the non-optimized sensor (Procedure-1: Preliminary), this initial purification step was not performed. After purification, the volume was adjusted to 6 mL. To proceed with functionalization, 300 µL of thiolated ssDNAprobe (200 µM) were added, and the suspension was incubated at 4°C overnight. At the end of the process, a total volume of 6.3 mL was obtained.

2.2.3. Purification of AuNCs-ssDNA

To remove the excess ss-DNA probe, a dialysis process with an 8-10 kDa membrane was performed, followed by ultrafiltration using centrifugal Amicon filter (3 kDa) to concentrate the sample. To activate the dialysis membrane, it was immersed in a water - 10% ethanol solution for 15 minutes under agitation. Subsequently, it was thoroughly washed with deionized water both internally and externally for 30 minutes under agitation. After activation, the ss-DNA probe was dialyzed against the MES buffer (50 mM, pH 6). A solution of 6.3 mL of ss-DNA probe was placed into the membrane and immersed in a beaker containing 200 mL of MES buffer. The external solution was replaced every 2 hours for a total of 3 hours, maintaining continuous agitation to ensure effective dialysis. After dialysis, the purification of the ss-DNA probe was completed using a centrifugal Amicon filter (3 kDa). The ss-DNA probe suspension was concentrated at 12,000 rpm for 7 minutes. Subsequently, the volume was adjusted back to 6.3 mL.

2.3. Characterization

2.3.1. Transmission electron microscopy (TEM)

Transmission electron microscopy analysis was carried out with a Jeol 2100 transmission electron microscope operated at 200 KV, supplied with UltraScan 1000XP CCD Camera. For sample preparation, 300-mesh carbon-coated nickel grids were placed for 1 min on top of a 40 μL sample droplet and dried up with paper. Particle sizes and interparticle distances were determined from TEM micrographs using Fiji Software.

2.3.2. Dynamic light scattering (DLS)

DLS measurements were carried out using a Zetasizer NanoZS90 (Malvern), with a laser set at 633 nm and a scattering angle of 90°. The temperature was set at 25°C, according to a Standard Operating Procedure (SOP).

2.3.3. UV-Vis measurements

were carried out using a Perkin Elmer 365 spectrophotometer with a quartz cuvette with a 10 mm optical path, in the wavelength range between 300 and 800 nm. To assess the stability of the AuNCs in different environments, equal volumes of the NCs suspension (after synthesis) and various buffers (PBS 1 ×, SSC 1 ×, TE 1 ×, MES 10 mM, and ultrapure water) were mixed and incubated overnight at 4 °C prior to measurement

2.3.4. Fluorescence measurements

were performed using a Fuoromax-3 Jobin Yvon Horiba spectrofluorometer, with a quartz cuvette with a 10 mm optical path and excitation set at 400 nm. The additional fluorescence measurements, under different pH conditions, were taken on the AuNCs suspension solution in water (initial pH 2.20) and at various pH (4.06, 5.21, 6.64, 7.96, 10.25, 11.36) by adding multiple aliquots of 20 μL NaOH 1 M.

2.3.5. Time-resolved measurements

were performed at room temperature using a Horiba Nanolog spectrofluorometer equipped with a pulsed nano-LED with a nominal emission peak at 370 nm. The decay curves were acquired over a 3.2 μs time window to ensure full decay collection. Lifetime values were obtained by fitting the decay profiles with a three-exponential function.

2.3.6. Luminescence excitation and emission 3D maps

The 3D fluorescence maps were obtained using a Horiba Nanolog spectrofluorometer at room temperature. The resolution of both the excitation and emission slits was set to 5 nm. A high-pass filter (500 nm) was used to block the excitation wavelength from the lamp. The acquisition time was set to 0.2 s. Maps were obtained for the suspension both in water and after the addition of MES.

2.3.7. Photoluminescence quantum yield (ϕ)

The Photoluminescence quantum yield (ϕ) of AuNCs, AuNCs-ssDNA and AuNCs-dsDNA dispersion in water (n=1.335) was calculated using the procedure described in supporting information.

2.3.8. Zeta potential measurements

were performed using the Zetasizer NanoZS90 (Malvern Instruments, UK) equipped with a He−Ne laser source ($\lambda = 633$ nm) at the scattering angle of 90°. The suspensions were loaded into disposable folded capillary cells (Zeta Cell, DTS 1060), and data were collected at 25°C.

2.3.9. FT-IR spectroscopy measurements

were performed with a JASCO FT/IR-4600 spectrometer equipped with an ATR accessory for powder diffusion mode. Samples were prepared by drop-casting 60 μL of AuNCs, AuNCs-ssDNA, and ssDNA suspensions onto silicon substrates and drying them at room temperature for 24 hours prior to analysis.

2.4. Sensor tests

2.4.1. Time-dependent hybridization study

To evaluate the time response of the sensor, a study was conducted on the hybridization of AuNCs-ssDNA with the complementary sequence of ss-DNA target. 150 μL of ss-DNA-target (100 μM) were added to 1.6 mL of AuNCs-ssDNA to reach a final target concentration of 10 μM. The fluorescence cuvette was sealed with parafilm and was not opened again, being incubated directly in the same cuvette. The suspension was incubated at 50°C, and UV-Vis and fluorescence measurements were taken every 15 minutes for 75 minutes to monitor the changes induced by hybridization.

2.4.2. Concentration-dependent hybridization study

To evaluate the sensor's response to different target concentrations, a series of DNA-target suspensions at increasing concentrations were prepared. Control measurements were also performed using nonspecific ssDNA under the same conditions. For each measurement, a fixed volume of 2 μL from these suspensions was added to 2 mL of the AuNCs-ssDNA suspension, and the resulting fluorescence quenching was recorded. The suspension was incubated at 40°C for 45 minutes with agitation at 400 rpm after each addition of target, to reach maximum hybridization as observed in the time-dependent study. The fluorescence cuvette was sealed with parafilm and incubated without being opened. After each addition, the suspension was allowed to cool for 15 minutes before measurement.

2.4.3. Analyte-specificity evaluation

To evaluate the specificity of the sensor, a study was conducted using different analytes, including glucose, glycine, and BSA (bovine serum albumin), each prepared at a final concentration of 3 nM. A suspension of 6.3 mL of AuNCs-ssDNA was diluted with MES buffer to a final volume of 9.3 mL. Subsequently, 5 μL of each analyte solution was added to 1.5 mL of the diluted suspension. Fluorescence was measured before the addition of the analyte and after incubation at 40°C for 45 minutes with agitation, followed by 15 minutes of cooling.

2.4.4. Sensor evaluation in blood matrix

A study was conducted to evaluate the sensor's performance in the presence of blood. A 3 mL volume of AuNCs-ssDNA after purification was split into two equal samples. In both, 2.5 μL of whole blood was added to 1.5 mL of the NCs suspension. In the test sample, 2.5 μL of complementary DNA (1 μM) was added; in the control sample, 2.5 μL of MES buffer (50 mM) was added instead. Fluorescence was first measured after the addition of blood to establish a baseline, and subsequently after each individual addition of DNA or MES aliquots. (2.5 μL at a time) to the test or control sample respectively. The blood volume remained constant in all samples. For each measurement, samples were incubated at 40°C for 45 minutes, followed by cooling at room temperature for 15 minutes before fluorescence recording.

3. Results and discussion

3.1. Nanoclusters synthesis and optical properties

Gold nanoclusters (AuNCs) were synthesized using an eco-friendly methodology without employing dangerous organic solvents, thus ensuring a low environmental impact. This method, previously reported in our studies,[33,34] allows the nanoclusters to be obtained in just three hours (Fig. 1a). Subsequently, the nanoclusters were characterized both morphologically and optically.

For the morphological characterization, Dynamic Light Scattering (DLS) was used, indicating a hydrodynamic diameter of about 3 nm (Fig. 1b). Additionally, Transmission Electron Microscopy (TEM) was performed, which allows for the observation of only the metallic core. TEM imaging enabled measurement of the NCs' diameters, resulting in

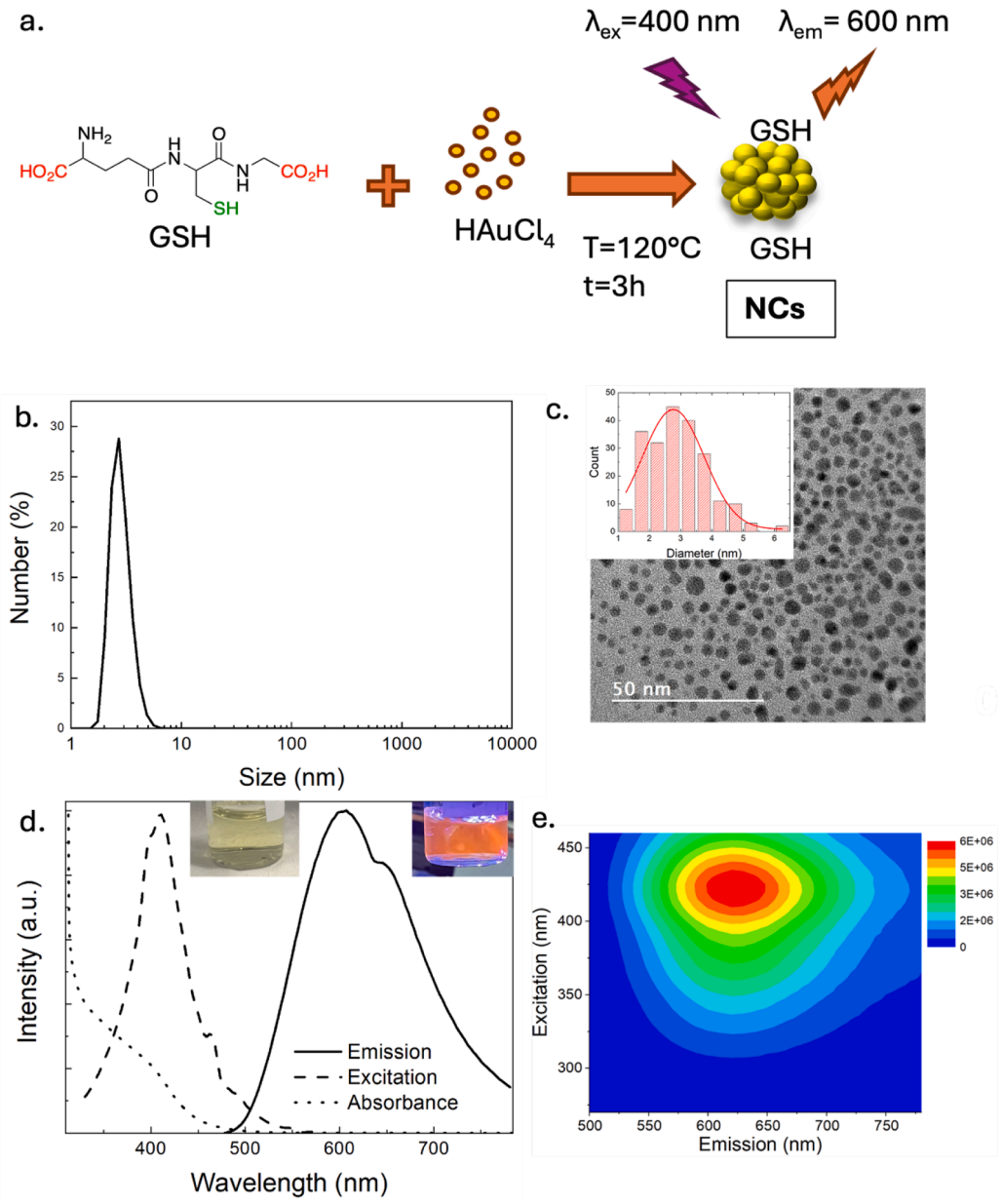

Fig. 1. Synthesisand Characterization of GSH AuNCs. a) Schematic of the synthesis of GSH gold nanoclusters (GSH Au NCs). Morphological characterization of the post-synthesis NCs by b) DLS and c) HR-TEM with the diameter distribution shown in the inset. Optical characterization of the post-synthesis NCs through d) UV-Vis absorbance spectrum and photoluminescence emission spectrum recorded with 400 nm excitation and excitation spectrum recorded at 600 nm emission. e) 3D photoluminescence map with emission wavelength as a function of excitation wavelength, with fluorescence intensity represented by different colors along the Z-axis.

an average core diameter of 2.7 ± 0.9 nm (Fig. 1c), consistent with the values reported in the literature for luminescent gold NCs. These results are coherent, as the DLS measurement considers the metallic core along with the ligand and hydration shell of the nanoclusters, leading to an overall larger diameter compared to that of the metallic core alone observed with TEM.

In addition to the morphological properties, the optical properties of the NCs were analyzed. UV-Vis absorbance analysis showed a diagnostic peak for gold NCs at around 400 nm, characteristic of these sizes. Subsequently, fluorescence studies were conducted, revealing a photoexcitation peak around 400 nm and an emission peak at 600 nm, with a shoulder at 650 nm (Fig. 1d).

Finally, to further characterize the optical properties of the nanoclusters, 3D excitation-emission maps were generated, providing a comprehensive view of the NCs' optical response as a function of different excitation and emission wavelengths (Fig. 1e).

3.2. *Nanoclusters functionalization*

To use these nanoclusters (NCs) as sensors for biological analytes, functionalization is required to enable selective recognition of the target molecules. For this purpose, thiolated ss-DNA was employed, which binds to gold and, via a ligand exchange process, replaces the GSH on the NCs surface (Fig. 2a). An excess of HS-ssDNA was added to the NCs suspension and incubated overnight at 4°C. The following day, unbound excess DNA was removed through ultrafiltration.

NCs functionalized with HS-ssDNA (AuNCs-ssDNA) tend to precipitate in water; the use of a buffer such as MES stabilizes the DNA structure, pH, and ionic strength, effectively preventing denaturation and precipitation while simulating the biological environment. We selected

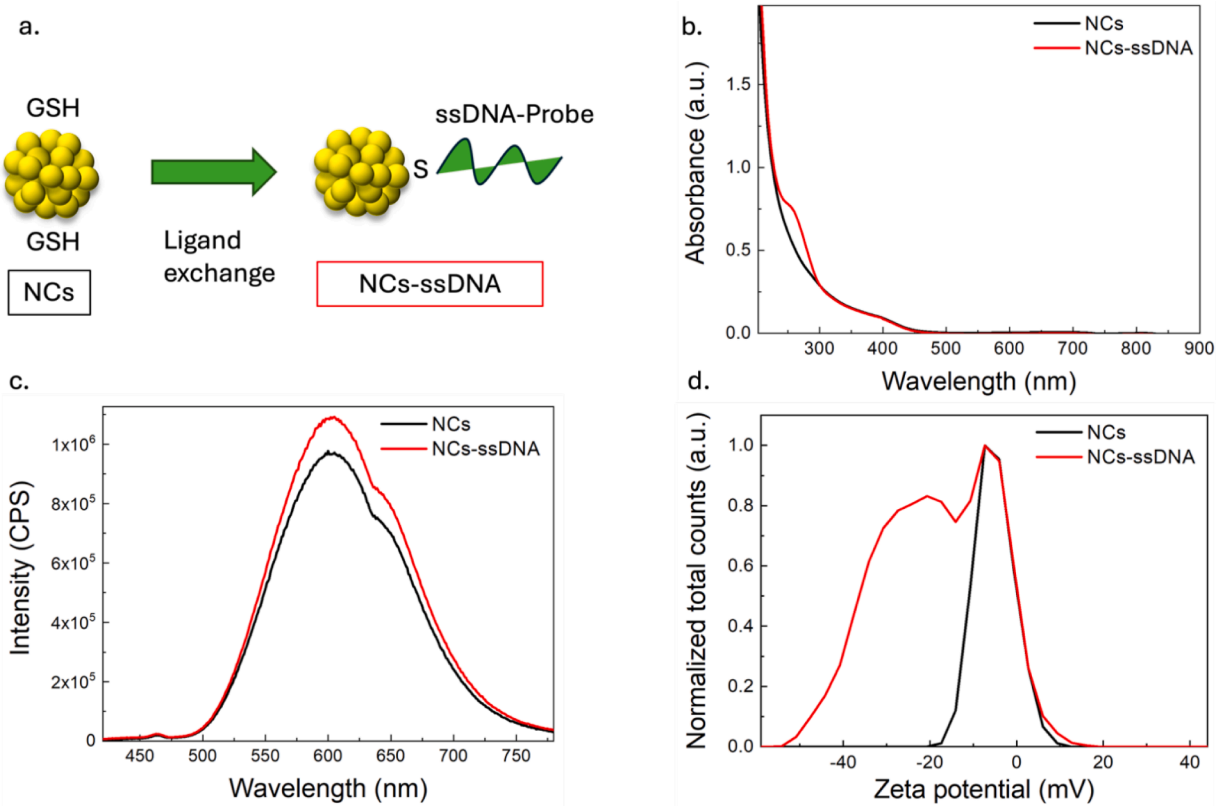

Fig. 2. Characterization of ssDNA-Functionalized AuNCs. a) Schematic of AuNCs-ssDNA ligand exchange with the HS-ssDNA probe. b) UV-Vis absorption spectrum c) Fluorescence spectrum (λ_{exc} = 400 nm) and d) Zeta potential measurement of the AuNCs before (black line) and after (red line) functionalization with the ssDNA probe.

MES buffer specifically because it preserves both DNA structure and AuNCs colloidal stability. In contrast, buffers such as PBS, SSC, and Tris-EDTA induced increased scattering, as seen in the rising UV-Vis background, which is indicative of nanoparticle aggregation. These results are shown in Supplementary Fig. S3d.

A 24-base probe was selected as a compromise between stability and efficiency: shorter sequences (<15 nt) may not hybridize efficiently due to lower thermodynamic stability and a higher risk of transient, nonspecific interactions, while longer sequences (>30 bases) are more prone to forming secondary structures, which could hinder hybridization or reduce quenching efficiency [35].

To confirm the ligand exchange and observe changes in the properties of the NCs after the addition of DNA, various characterization analyses were performed. The UV-Vis absorbance spectrum shows a peak at 260 nm, corresponding to the absorption of the nucleic acids in DNA. This peak remains even after purification, indicating that the DNA has been successfully attached to the NCs (Fig. 2b). This finding is further supported by FT-IR spectroscopy (Supplementary Fig.s S1 and S2), which highlights spectral changes consistent with ligand substitution and the presence of DNA-specific vibrational bands. In particular, the ATR spectra of the AuNCs-ssDNA suspensions show shifts in comparison to the reference peaks of ssDNA: 3234 cm^{-1} (C–H, N–H, O–H stretching), 1689 cm^{-1} (C=O stretching of guanine), 1643 cm^{-1} (C=O stretching of cytosine), 1000 cm^{-1} (P–O/C–O stretching in deoxyribose), and 921–910 cm^{-1} (C–C stretching in deoxyribose). The presence and shifts of these peaks confirm the effective binding between AuNCs and ssDNA.

To verify that the functionalization process does not alter the NCs core structure, additional TEM analysis was performed after DNA attachment. The images show no appreciable changes in core morphology or aggregation, confirming structural preservation after ligand exchange (Supplementary Fig. S3a).

Additionally, fluorescence analysis shows that, at the same AuNCs concentration (and corresponding absorbance at 400 nm), the intensity of the emission peak at 600 nm increases after ligand exchange with ssDNA, indicating an enhanced quantum yield (Fig.2c). The photoluminescence quantum yield (QY) of AuNCs in water was measured before and after functionalization with ssDNA. The QY increased significantly from 0.012 to 0.069, confirming that the ligand exchange with ssDNA improves the emission efficiency of the nanoclusters (see Supporting Information). This enhancement in QY may be attributed to several factors. Longer and more rigid ligands such as ssDNA can reduce non-radiative decay pathways and enhance charge transfer efficiency, as also reported in previous studies [6,36]. Moreover, the DNA shell likely acts as a protective barrier, reducing energy loss to the surrounding environment and improving the overall photoluminescence performance of the nanoclusters.

It is worth noting that no shift in the emission wavelength was observed following functionalization. This behavior is expected, as the emission of AuNCs is primarily determined by the size and structure of the metallic core, while surface ligands typically influence excitation efficiency and quantum yield rather than the emission position [37].

Additional photophysical characterization, including pH-dependent PL intensity, lifetime decay analysis, and sensor stability in different buffer conditions, is shown in Supplementary Fig. S3. The sensor also demonstrated excellent stability over time, showing only ~10% decrease in fluorescence intensity after 12 days in MES buffer, with no spectral changes (Supplementary Fig. S4).

For further verification of probe attachment, the zeta potential of the nanoparticles was measured both before and after ssDNA functionalization. The zeta potential provides information about the surface charge of the nanoparticles, and its variation is indicative of ssDNA attachment. A significant change in zeta potential suggests that the ssDNA has successfully bound to the surface of the NCs, modifying their surface charge. The results show a zeta potential value of -7 mV for GSH-capped

NCs and a more negative value of -20 mV after ssDNA attachment (Fig. 2d).

3.3. Analyte recognition kinetic study

After preparing the NCs with the probe, the suspension was exposed to target DNA (ssDNA-target), and fluorescence variations in response to the analyte were measured (Fig. 3a).

To monitor fluorescence changes during hybridization, the fluorescence signal of the NCs was measured every 15 minutes of incubation, monitoring the process and allowing the identification of the stabilization point. A progressive decrease in fluorescence signal (quenching) was observed at each 15-minute interval, stabilizing after approximately one hour of incubation (Fig. 3b). This time corresponds to the period typically required for the complete hybridization of the two DNA strands, as the process requires enough interactions between complementary bases to form a stable bond [38].

These results suggest that the fluorescence of the NCs is sensitive to the presence of the ssDNA-target and is progressively quenched as the target binds to the probe (Fig. 3c). This quenching effect may be attributed to a decrease in ligand-to-metal charge transfer (LMCT), which plays a central role in AuNCs fluorescence. Upon hybridization, some of the electrons involved in the LMCT process may become more tightly bound within the double-stranded DNA structure, thereby reducing the efficiency of charge transfer to the gold core and leading to diminished emission [39]. Further insight into the interaction between the sensor and the target was obtained through time-resolved photoluminescence measurements (Supplementary Fig. S3c and Table S2). The fluorescence decay was fitted using a three-exponential model, revealing an increase in all three lifetime components (τ_1, τ_2, and τ_3) upon DNA functionalization and subsequent hybridization. The intensity-weighted average lifetime also shows a progressive enhancement, increasing from 9 ns for GSH NCs to 226 ns after DNA functionalization and to 1 μs following target hybridization. This trend is consistent with a reduction in non-radiative decay pathways, and may suggest that target hybridization leads to a more rigid and stabilized nanocluster environment, potentially due to restriction of molecular motion upon duplex formation.

Fig.s S5 and S6 provide detailed insights into the fluorescence variations of the NCs, influenced by the buffer composition and their functionalization with the ssDNA-probe and ssDNA-target.

3.4. Sensor performance

To evaluate the effectiveness of the functionalized NCs as a sensor, different target concentrations were studied. The goal is to correlate the quenching intensity with the target concentration in solution (Fig. 4a). Increasing target concentrations were incubated for one hour each, a duration identified in the previous section as sufficient to ensure complete hybridization saturation. It is worthy of note that the quantum yield (QY), calculated as described in SI, shows only a modest decrease upon target addition from 0.069 to 0.061 (Table S1). While this variation is relatively small, indicating general stability of the system, it is consistent with the fluorescence quenching effect expected from hybridization with the complementary DNA sequence.

The quenching intensity as a function of target concentration was fitted using the Hill equation (Eq. (1)), which describes the relationship between analyte concentration and system response in cooperative binding processes [40,41].

$$Y = \frac{V_{max}}{1 + (Kd/x)^n} \quad (1)$$

In this equation V_{max} represents the maximum quenching intensity, K_d is the dissociation constant indicating the concentration at half-maximal response, and n is the Hill coefficient, which reflects binding cooperativity. The fitting revealed a Kd of 1.6 ± 1.0 nM, indicating the sensor's ideal working range, and a n value of 0.74 ± 0.32, suggesting anti-cooperative binding. The maximum quenching reached at 693 nM of 25%, with a detection limit (LOD) of 32 pM, highlight the sensor's high sensitivity. The LOD was calculated using the inverse function of the Hill equation, considering the concentration corresponding to a signal three times the noise (see SI) [42].

To verify the specificity of the binding, a test was performed by incubating the sensor with nonspecific DNA. This control experiment is important to demonstrate that the sensor responds selectively to the specific target and not to similar but non-complementary DNA sequences. In this case as well, quenching was observed, but with lower saturation values, indicating a less intense response compared to the specific target (Fig.4b). The specificity of the sensor will be discussed in Section 3.6.

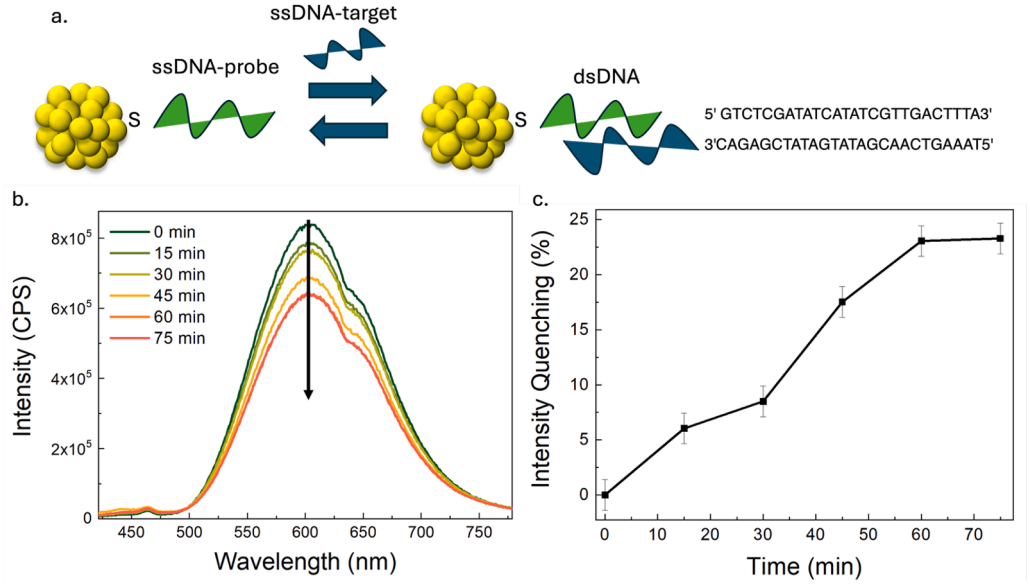

Fig. 3. Time-Dependent Hybridization Study. a) Schematic representation of the interaction equilibrium between the two DNA strands of the sensor in the presence of specific DNA. b,c) Kinetic fluorescence analysis of the sensor in the presence of a fixed concentration of ssDNA target (10 μM). b) Fluorescence spectra at various incubation times and c) percentage quenching intensity of the sensor over time relative to its initial fluorescence intensity (λexc = 400 nm, λem = 600 nm).

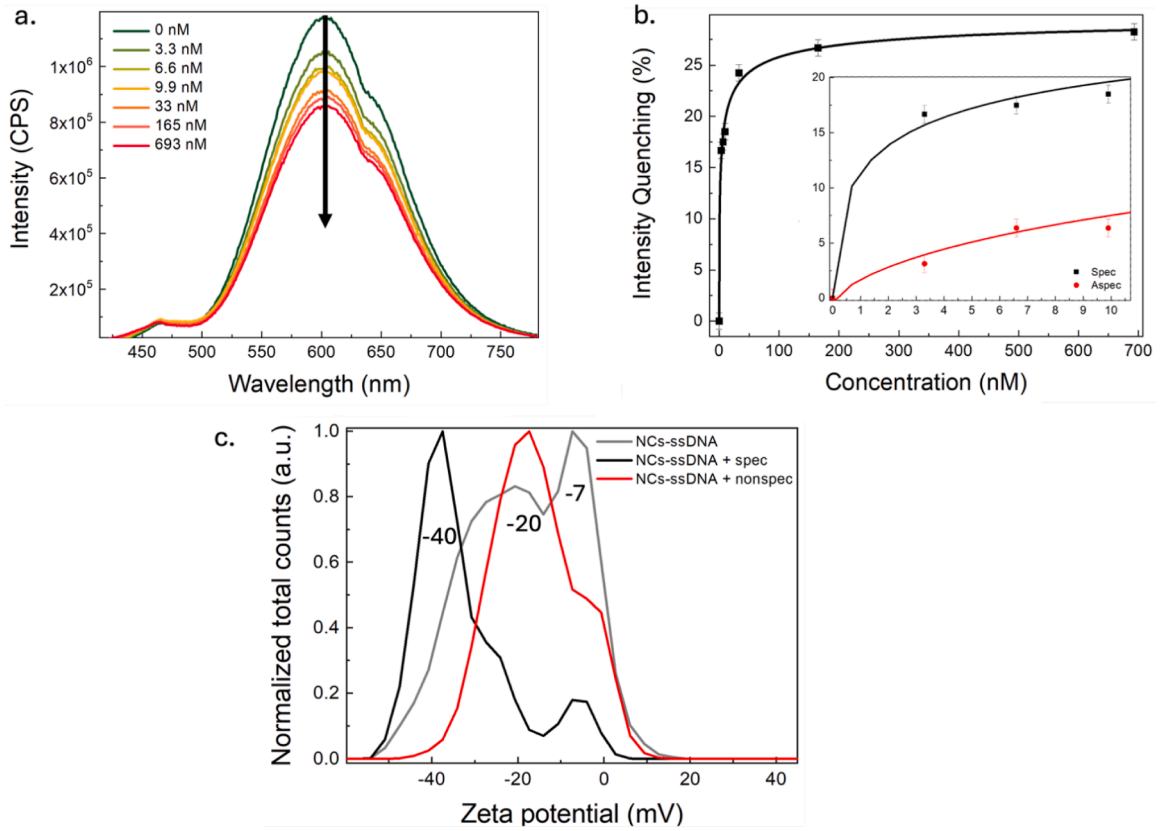

Fig. 4. Concentration-Dependent Hybridization Study. a) Fluorescence spectrum of the sensor incubated with different concentrations of ssDNA target. b) Percentage of quenching intensity of the sensor in the presence of increasing target concentrations relative to the initial fluorescence intensity, with a comparison between specific and nonspecific ssDNA in the inset (λexc = 400 nm, λem = 600 nm). c) Zeta potential measurement of the sensor in the absence and presence of specific and nonspecific ssDNA.

To confirm the effective binding of the complementary target compared to the nonspecific one, a zeta potential study was conducted. The zeta potential provides information about the surface charge of the nanoparticles, allowing for the evaluation of surface changes related to target adsorption. A significant variation in zeta potential indicates that the specific target has successfully bound, altering the surface charge of the NCs. Our study showed a decrease in zeta potential from -20 mV (with only the probe) to -40 mV in the presence of the specific target, while the zeta potential remained stable at -20 mV in the presence of nonspecific DNA (Fig. 4c). The initial shift from –7 mV (GSH-capped NCs) to –20 mV after ssDNA functionalization reflects the attachment of negatively charged phosphate groups from the single-stranded DNA, confirming successful ligand exchange. Upon hybridization with the complementary target, the further decrease to –40 mV is attributed to the formation of a double-stranded DNA, which increases the overall surface charge density and enhances electrostatic repulsion. This contributes to improved colloidal stability by preventing aggregation in complex environments, while simultaneously confirming the occurrence of specific target recognition. In contrast, the zeta potential remains unchanged in the presence of nonspecific DNA, indicating the absence of stable hybridization and reinforcing the selectivity of the sensor.

3.5. Sensor optimization

To enhance the sensitivity of the sensor and decrease its LOD, the sensor was optimized by increasing the amount of probe attached to the surface of the NCs. Initially, the ligand exchange with ssDNA-probe was performed directly on AuNCs without any pre-purification (Procedure-1: Preliminary). However, to improve the process, a new approach was adopted (Procedure-2: Optimized), where the NCs underwent a pre-purification step to remove excess GSH before performing the ligand exchange with the ssDNA probe. This pre-purification allowed for a more efficient ligand exchange, as the ssDNA probe in Procedure-2 is present in a greater excess compared to the Procedure-1, significantly increasing the amount of probe on the surface and enhancing the sensor's performance.

UV-Vis absorption spectra were measured for both the AuNCs-ssDNA sensors (Procedure-1 and 2) to evaluate the effectiveness of the improvement in functionalization and determine the amount of DNA bound to the surface. A higher peak at 260 nm was observed for the AuNCs-ssDNA prepared by the optimized Procedure-2, indicating a greater amount of probe on the surface of the NCs. (Fig. 5a). The amount of ssDNA anchored at AuNCs was calculated as described in SI. The results demonstrate a significant improvement, with approximately 34% more ssDNA anchored when using the optimized Procedure-2 compared to Procedure-1.

Table 1 presents the absorbance values at 260 nm for the AuNCs without the probe and for AuNCs-ssDNA with two different probe concentrations, both before and after sensor optimization.

The detection capability of the sensor prepared with the two procedures was also compared, showing higher quenching for the sensor with a greater amount of probe, at the same analyte concentration (Fig. 5b). The performance of the Optimized sensor is better illustrated in Fig. S7. Higher quenching is advantageous for detection as it indicates greater sensor sensitivity. Table 2 reports the fitting parameters of the sensors prepared according to the two procedures, including the dissociation constant, Hill coefficient, saturation value, and sensor LOD, to provide a detailed comparison. With a greater amount of probe on the NC surface, the dissociation constant decreases. This indicates a higher affinity for the analyte, allowing the sensor to operate at lower

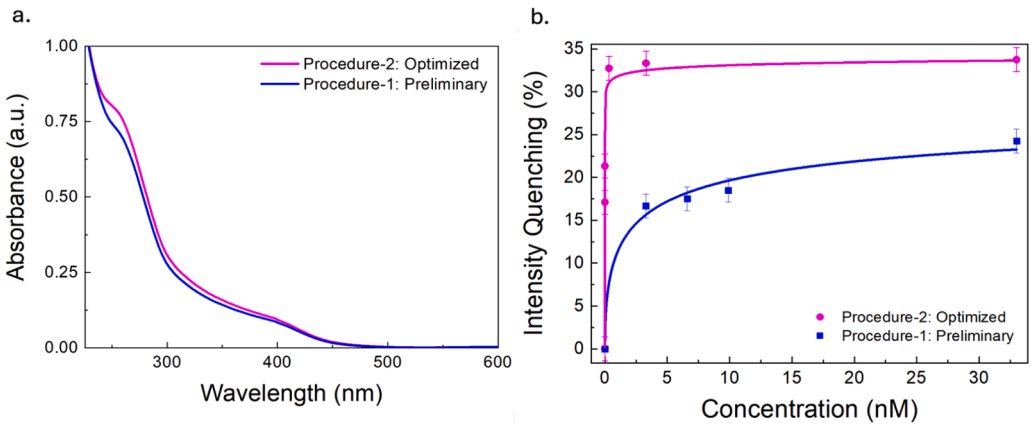

Fig. 5. Sensor Optimization. Comparison between the sensor with less ss-DNA probe (blue line) and the optimized sensor with more probe on the surface (magenta line) through a) UV-Vis absorption spectrum and b) percentage of fluorescence quenching intensity as a function of increasing ss-DNA target concentration (λ_{exc} = 400 nm, λ_{em} = 600 nm).

Table 1
Absorbance values of AuNCs in the absence and presence of ssDNA probe on the surface, for the sensor before (Procedure-1) and after (Procedure-2) optimization, to estimate the concentration of ssDNA probe on the sensor surface.

	AuNCs	AuNCs-ssDNA Procedure-1: Preliminary	AuNCs-ssDNA Procedure-2: Optimized
A@260 nm	0.5181	0.6933	0.7545
Conc DNA (μM)	0	0.70	0.94

Table 2
Summary of fitting parameters obtained from the Hill model for fluorescence quenching in the presence of specific DNA, comparing the sensor before (Procedure-1) and after (Procedure-2) optimization. (λexc = 400 nm, λem = 600 nm). Vmax indicates the maximum quenching intensity at saturation, Kd is the dissociation constant, n is the Hill coefficient reflecting the cooperativity of the binding process, and LOD is the limit of detection.

AuCNS-ssDNA (Procedure-1: Preliminary)	AuCNS-ssDNA (Procedure-2: Optimized)
Kd = 1.6 ± 1.0 nM	Kd = 79.3 ± 5.0 fM
n = 0.74 ± 0.32	n = 0.40 ± 0.02
Vmax: 25 %	Vmax: 34 %
LOD = 32 pM	LOD = 25 aM

concentrations. A lower dissociation constant is advantageous because it improves sensor sensitivity, as also reflected by a significantly lower LOD (at the attomolar level).

3.6. Specificity test

To evaluate the specificity of the sensor, several tests were conducted, including the comparison between specific and nonspecific DNA, the addition of other analytes, and exposure to biological fluids. Fig. 6a shows the fluorescence quenching as a function of DNA concentration. A logarithmic scale was used to cover the wide range of concentrations tested, spanning several orders of magnitude. In this study, the sample was divided into three equal aliquots to test quenching in response to different additions: specific ssDNA, nonspecific ssDNA, and only buffer (MES). This approach allows for evaluating the sensor's specificity to different types of interactions.

Although quenching is also observed with nonspecific DNA, it is of lower intensity compared to specific DNA. The same test conducted with the addition of only buffer shows quenching similar to that observed with nonspecific DNA. This result suggests that the quenching observed in the presence of nonspecific DNA is not due to specific recognition by the sensor, but rather to the intrinsic sensitivity of the nanoclusters to the buffer environment. Since the same small volume (2 μL) was added to each sample, with a total volume of 2 mL, the dilution effect is negligible. Sensitivity to the buffer is relevant because it demonstrates that the sensor also responds to environmental changes, highlighting the importance of careful analysis of the response to avoid false positives. This indicates that NCs are highly sensitive to variations in the surrounding environment but exhibit more pronounced quenching only in the presence of specific DNA.

Additional specificity experiments have been performed using analytes, such as bovine serum albumin (BSA), glucose, and glycine, at the maximum concentration used for the sensor (3 nM). These analytes were chosen to represent different types of common biological molecules (protein, carbohydrate and amino acids), to evaluate the specificity of the sensor and its response to potential interferents present in a biological environment. In these cases as well, greater quenching was observed with specific-DNA (Fig. 6b).

To evaluate the sensor's effectiveness directly in biological fluids, untreated human blood sampled by finger prick was added to the nanocluster suspension. The sample was divided into two equal parts: specific-DNA was added to the first, while only buffer (MES) was added to the second. Despite the complexity of the matrix, the sample with specific DNA showed quenching three times greater than the sample with only buffer, demonstrating the sensor's effectiveness even in a biological environment (Fig. 6c). The presence of blood introduces proteins and other components that can interfere with the sensor signal, making detection more challenging and simulating real usage conditions.

After the addition of blood, the NCs sample without specific DNA showed visible aggregation during incubation, unlike the sample containing the complementary target. This effect is attributed to the stabilizing role of the DNA probe, which provides electrostatic repulsion and steric hindrance at the NC surface, mitigating non-specific interactions with blood proteins and other biomolecules that typically reduce zeta potential and induce aggregation. The hybridization with the target sequence further reinforces this protective effect, enhancing the colloidal stability of the nanoclusters even in a complex biological matrix.

The inset of Fig. 6c highlights the aggregates observed in the sample lacking specific DNA, compared to those in the presence of specific DNA; this effect was also confirmed through UV-Vis absorption measurements (Fig. 6d). UV-Vis measurements allow monitoring of light scattering caused by aggregates, providing an indication of the presence of aggregation and the stability of the sample. In this graph, the sample to

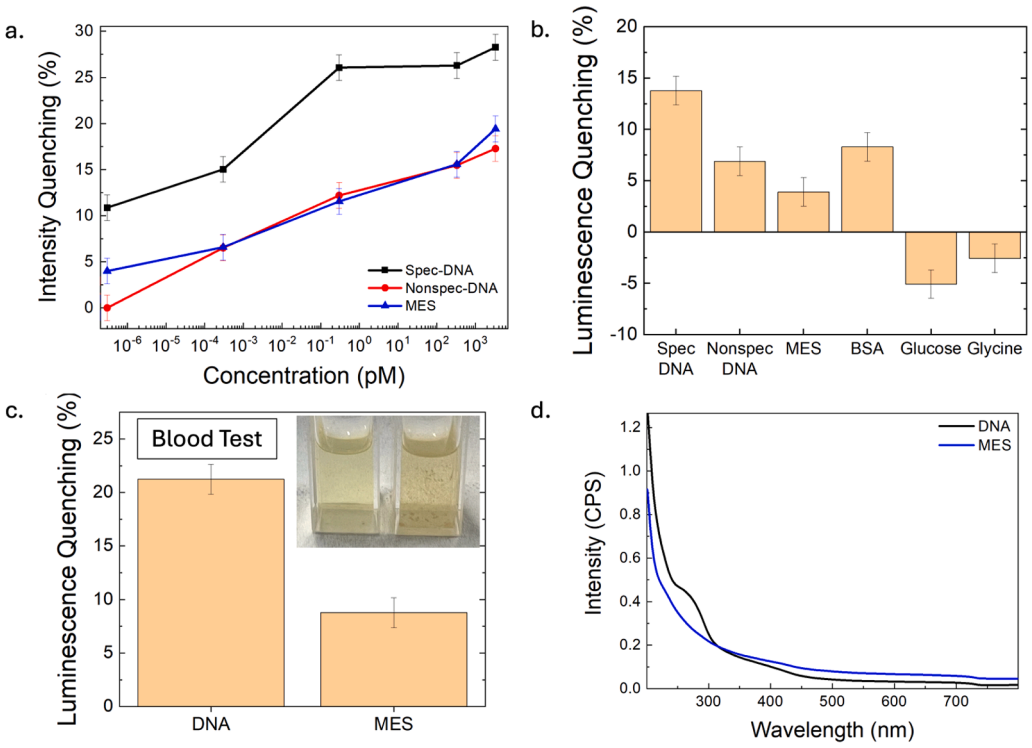

Fig. 6. Sensor analyte specificity and evaluation in blood matrix. a) Percentage quenching intensity as a function of concentration in logarithmic scale for the sensor in the presence of specific ssDNA (black line), nonspecific ssDNA (red line), and MES buffer only (blue line). b) Percentage quenching intensity of sensor luminescence in the presence of different analytes at a constant analyte concentration (3 nM). c) Percentage quenching intensity of sensor luminescence in blood matrix in the presence of specific ssDNA in MES (3 nM) and MES buffer only (λexc = 400 nm, λem = 600 nm), inset photographs of sensor in blood with specific-DNA (left) and MES (right). d) UV-Vis absorption curve of the sensor in blood matrix in the presence of specific-DNA (black line) and MES buffer only (blue line).

which only MES was added presents a higher scattering background. The typical peaks of the NCs and DNA are no longer present, as most of the NCs aggregated and precipitated to the bottom of the cuvette. Conversely, the sample with specific DNA appears clear, with a spectrum showing the peak at 400 nm, typical of NCs, and the peak at 260 nm, characteristic of DNA, similar to the spectrum of the sensor before the addition of blood.

4. Conclusions

This study demonstrated the successful synthesis and functionalization of gold nanoclusters (NCs) to develop an ultrasensitive, eco-friendly, and label-free sensor. The synthesis of NCs was performed using environmentally friendly methods without organic solvents, and the resulting NCs exhibited excellent optical properties, with an absorbance peak at 400 nm and an emission peak at 600 nm. After the NCs functionalization with thiolated ss-DNA, the luminescence intensity increased, indicating an enhancement in quantum yield passing from 0.012 to 0.069. Kinetic studies demonstrated that the sensor could detect fluorescence changes in response to target interaction, confirming its reliability in monitoring the hybridization of specific DNA. Sensor performance was further evaluated by comparing the response to different concentrations of analyte. Optimization of the sensor, by increasing the probe amount on the NCs surface by 34%, further improved performance, enhancing sensitivity to lower analyte concentrations. This optimization enabled a significant improvement in the limit of detection (LOD), shifting from the picomolar to the attomolar range. The specificity test confirmed the sensor's ability to distinguish between specific and nonspecific DNA, showing specificity even in complex biological fluids such as blood.

Although this study focused on fully mismatched sequences, future work will address the sensor's ability to detect single-nucleotide mismatches. Despite the relatively low quantum yield of AuNCs, the sensor achieves high sensitivity through an efficient quenching mechanism and operates without amplification, labeling, or enzymes offering a simpler and more sustainable alternative to conventional methods. Further efforts will aim to improve surface passivation, investigate the effect of probe design on sensor performance, and extend the platform to detect proteins or small molecules via aptamers or peptides.

This result, combined with the eco-friendly synthesis and label-free nature of the sensor, demonstrates the effectiveness of the developed system as a highly sensitive tool for detecting biological analytes. Additionally, the platform is easily adaptable to different biological analytes through the addition of specific aptamers, making it promising for medical diagnostics and environmental monitoring applications. The simplicity of the synthesis, specificity and sensitivity of the developed sensor make it a promising technology for future development in real and complex settings.

CRediT authorship contribution statement

Regina Maria Chiechio: Writing – original draft, Project administration, Methodology, Investigation, Formal analysis, Data curation, Conceptualization. **Antonino Scandurra:** Writing – review & editing, Investigation. **Riccardo Reitano:** Investigation. **Paolo Musumeci:** Investigation. **Maria Grazia Grimaldi:** Investigation. **Annalinda Contino:** Writing – review & editing, Investigation. **Giuseppe Maccarrone:** Investigation. **Valerie Marchi:** Writing – review & editing, Investigation. **Ludovica Maugeri:** Methodology, Investigation, Data curation. **Salvatore Petralia:** Writing – review & editing, Validation, Supervision, Methodology, Conceptualization. **Francesco Ruffino:** Writing – review & editing, Investigation, Funding acquisition.

Declaration of competing interest

The authors declare the following financial interests/personal relationships which may be considered as potential competing interests:

Francesco Ruffino reports financial support was provided by Ministry of Education and Merit. If there are other authors, they declare that they have no known competing financial interests or personal relationships that could have appeared to influence the work reported in this paper.

Acknowledgements

The work was supported by PNRR MUR project PE0000023-NQSTI the PNRR NQSTI "National Quantum Science and Technology Institute" 1 Spoke 7.

Francesco Ruffino, Maria Grazia Grimaldi, Paolo Musumeci, Salvatore Petralia, Regina Chiechio thank the support by the project MhyNano "Multifunctional Hybrid Nanomaterials for Cancer Diagnosis and Personalized Target Therapy" through Programma di Ricerca di Ateneo UNICT 2024-26 linea 1.

Supplementary materials

Supplementary material associated with this article can be found, in the online version, at doi:10.1016/j.apsadv.2025.100762.

Data availability

Data will be made available on request.

References

[1] Komal Sonia, S. Kukreti, M. Kaushik, Gold nanoclusters: an ultrasmall platform for multifaceted applications, Talanta 234 (2021) 122623, https://doi.org/10.1016/j.talanta.2021.122623.

[2] E. Porret, X. Le Guével, J.-L. Coll, Gold nanoclusters for biomedical applications: toward *in vivo* studies, J. Mater. Chem. B 8 (11) (2020) 2216–2232, https://doi.org/10.1039/C9TB02767J.

[3] D. Hao, X. Zhang, R. Su, Y. Wang, W. Qi, Biomolecule-protected gold nanoclusters: synthesis and biomedical applications, J. Mater. Chem. B 11 (23) (2023) 5051–5070, https://doi.org/10.1039/D3TB00651D.

[4] Y. Zhang, C. Zhang, C. Xu, X. Wang, C. Liu, G.I.N. Waterhouse, Y. Wang, H. Yin, Ultrasmall Au nanoclusters for biomedical and biosensing applications: a mini-review, Talanta 200 (2019) 432–442, https://doi.org/10.1016/j.talanta.2019.03.068.

[5] T.-Q. Yang, B. Peng, B.-Q. Shan, Y.-X. Zong, J.-G. Jiang, P. Wu, K. Zhang, Origin of the photoluminescence of metal nanoclusters: from metal-centered emission to ligand-centered emission, Nanomaterials 10 (2) (2020) 261, https://doi.org/10.3390/nano10020261.

[6] Y. Huang, L. Fuksman, J. Zheng, Luminescence mechanisms of ultrasmall gold nanoparticles, Dalton. Trans. 47 (18) (2018) 6267–6273, https://doi.org/10.1039/C8DT00420J.

[7] Y. Lin, P. Charchar, A.J. Christofferson, M.R. Thomas, N. Todorova, M.M. Mazo, Q. Chen, J. Doutch, R. Richardson, I. Yarovsky, M.M. Stevens, Surface dynamics and ligand–core interactions of quantum sized photoluminescent gold nanoclusters, J. Am. Chem. Soc. 140 (51) (2018) 18217–18226, https://doi.org/10.1021/jacs.8b04436.

[8] D. Bain, S. Maity, T. Debnath, A.K. Das, A. Patra, Luminescent Au_6 and Au_8 nanoclusters from ligand induced etching of Au nanoparticles, Mater. Res. Express. 6 (12) (2019) 124004, https://doi.org/10.1088/2053-1591/ab5c8b.

[9] A. Kim, C. Zeng, M. Zhou, R. Jin, Surface engineering of Au_{36} $(SR)_{24}$ nanoclusters for photoluminescence enhancement, Part amp; Part Syst Charact 34 (8) (2017) 1600388, https://doi.org/10.1002/ppsc.201600388.

[10] R.M. Chiechio, S. Ducarre, C. Marets, A. Dupont, P. Even-Hernandez, X. Pinson, S. Dutertre, F. Artzner, P. Musumeci, C. Ravel, M.J.L. Faro, V. Marchi, Encapsulation of luminescent gold nanoclusters into synthetic vesicles, Nanomaterials 12 (21) (2022) 3875, https://doi.org/10.3390/nano12213875.

[11] E. Butera, A. Dupont, A. Aimé, S. Ducarre, R.M. Chiechio, P. Even-Hernandez, A. Contino, G. Maccarone, C. Ravel, V. Marchi, *In situ* labeling of the aqueous compartment of extracellular vesicles with luminescent gold nanoclusters, ACS. Appl. Mater. Interfaces. 16 (17) (2024) 21643–21652, https://doi.org/10.1021/acsami.4c02445.

[12] S. Zhu, X. Wang, Y. Cong, L. Li, Regulating the optical properties of gold nanoclusters for biological applications, ACS. Omega 5 (36) (2020) 22702–22707, https://doi.org/10.1021/acsomega.0c03218.

[13] L. Yang, P. Hou, J. Wei, B. Li, A. Gao, Z. Yuan, Recent advances in gold nanocluster-based biosensing and therapy: a review, Molecules. 29 (7) (2024) 1574, https://doi.org/10.3390/molecules29071574.

[14] D. Gopalan, A. Pandey, A.T. Alex, G. Kalthur, S. Pandey, N. Udupa, S. Mutalik, Nanoconstructs as a versatile tool for detection and diagnosis of Alzheimer biomarkers, Nanotechnology. 32 (14) (2021) 142002, https://doi.org/10.1088/1361-6528/abcdcb.

[15] M.A. Messina, L. Maugeri, G. Spoto, R. Puccio, M. Ruggieri, S. Petralia, Fully integrated point-of-care platform for the self-monitoring of phenylalanine in finger-prick blood, ACS. Sens. 8 (11) (2023) 4152–4160, https://doi.org/10.1021/acssensors.3c01384.

[16] L. Maugeri, G. Fangano, A. Ferlazzo, G. Forte, A. Gulino, S. Petralia, A DNA biosensor integrating surface hybridization, thermo-responsive coating, laminar-flow technology and localized photothermal effect for efficient electrochemical detection of nucleic acids, Sens. Diagn. (2024), https://doi.org/10.1039/D4SD00288A, 10.1039.D4SD00288A.

[17] P. Alpuim, E. Pinzón, L.C. Lopes, T. Domingues, J. Borme, E. Godoy, M.M. M. Raposo, P.R. Bueno, Molecular characterization and DNA-sensing using graphene electrochemical devices under illumination, in: 2023 IEEE Nanotechnology Materials and Devices Conference (NMDC), IEEE, Paestum, Italy, 2023, pp. 571–572, https://doi.org/10.1109/NMDC57951.2023.10344074.

[18] J.M. Lim, R. Tevatia, R.F. Saraf, Quantitative PCR of small nucleic acids: size matters, ChemistrySelect. 6 (12) (2021) 2975–2979, https://doi.org/10.1002/slct.202100807.

[19] B.A. Kairdolf, A.M. Smith, T.H. Stokes, M.D. Wang, A.N. Young, S. Nie, Semiconductor quantum dots for bioimaging and biodiagnostic applications, Annu. Rev. Anal. Chem 6 (1) (2013) 143–162, https://doi.org/10.1146/annurev-anchem-060908-155136.

[20] H. Nasrollahpour, B.J. Sánchez, M. Sillanpää, R. Moradi, Metal nanoclusters in point-of-care sensing and biosensing applications, ACS. Appl. Nano Mater. 6 (14) (2023) 12609–12672, https://doi.org/10.1021/acsanm.3c01569.

[21] R. He, S. Wang, F. Ju, Z. Huang, Y. Gao, J. Zhang, N. He, L. Nie, Metal nanocluster-based biosensors for DNA detection, Biosensors 15 (2) (2025) 72, https://doi.org/10.3390/bios15020072.

[22] L. Zhang, W. Su, S. Liu, C. Huang, B. Ghalandari, A. Divsalar, X. Ding, Recent progresses in electrochemical DNA biosensors for MicroRNA detection, Phenomics. 2 (1) (2022) 18–32, https://doi.org/10.1007/s43657-021-00032-z.

[23] S. Mussa Farkhani, P. Dehghankelishadi, A. Refaat, D. Veerasikku Gopal, A. Cifuentes-Rius, N.H. Voelcker, Tailoring gold nanocluster properties for biomedical applications: from sensing to bioimaging and theranostics, Prog. Mater. Sci. 142 (2024) 101229, https://doi.org/10.1016/j.pmatsci.2023.101229.

[24] L.-Y. Chen, C.-W. Wang, Z. Yuan, H.-T. Chang, Fluorescent gold nanoclusters: recent advances in sensing and imaging, Anal. Chem. 87 (1) (2015) 216–229, https://doi.org/10.1021/ac503636j.

[25] X.-J. Li, Y. Li, A.-Y. Liu, Y.-H. Tan, J. Ling, Z.-T. Ding, Q.-E. Cao, Highly selective visual sensing of copper based on fluorescence enhanced glutathione-Au nanoclusters, Spectrochim. Acta A: Mol. Biomol. Spectrosc. 224 (2020) 117472, https://doi.org/10.1016/j.saa.2019.117472.

[26] N.-Y. Hsu, Y.-W. Lin, Microwave-assisted synthesis of bovine serum albumin–Gold nanoclusters and their fluorescence-quenched sensing of Hg^{2+} ions, New. J. Chem. 40 (2) (2016) 1155–1161, https://doi.org/10.1039/C5NJ02263K.

[27] G. Zhang, Y. Li, J. Xu, C. Zhang, S. Shuang, C. Dong, M.M.F. Choi, Glutathione-protected fluorescent gold nanoclusters for sensitive and selective detection of Cu2+, Sens. Actuators B: Chem. 183 (2013) 583–588, https://doi.org/10.1016/j.snb.2013.04.023.

[28] J. Peng, L.-N. Feng, K. Zhang, X.-H. Li, L.-P. Jiang, J.-J. Zhu, Calcium carbonate–Gold nanocluster hybrid spheres: synthesis and versatile application in immunoassays, Chem. – Eur. J. 18 (17) (2012) 5261–5268, https://doi.org/10.1002/chem.201102876.

[29] Y. Wang, S. Wang, C. Lu, X. Yang, Three kinds of DNA-directed nanoclusters cooperating with graphene oxide for assaying mucin 1, carcinoembryonic antigen and cancer Antigen 125, Sens. Actuators B: Chem. 262 (2018) 9–16, https://doi.org/10.1016/j.snb.2018.01.235.

[30] J.-G. You, W.-L. Tseng, Peptide-induced aggregation of glutathione-capped gold nanoclusters: A new strategy for designing aggregation-induced enhanced emission probes, Anal. Chim. Acta 1078 (2019) 101–111, https://doi.org/10.1016/j.aca.2019.05.069.

[31] H.-B. Wang, Y. Li, H.-Y. Bai, Y.-M. Liu, DNA-templated Au nanoclusters and MnO2 sheets: A label-free and universal fluorescence biosensing platform, Sens. Actuators B: Chem. 259 (2018) 204–210, https://doi.org/10.1016/j.snb.2017.12.048.

[32] Y.S. Borghei, M. Hosseini, M.R. Ganjali, Oxidase-like catalytic activity of cys-AuNCs upon visible light irradiation and its application for visual miRNA detection, Sens. Actuators B: Chem. 273 (2018) 1618–1626, https://doi.org/10.1016/j.snb.2018.07.061.

[33] R.M. Chiechio, R. Le Guevél, S. Ducarre, H. Solhi, S. Dutertre, X. Pinson, J.-P. Bazureau, O. Mignen, P. Even-Hernandez, P. Musumeci, C. Ravel, M.J. Lo Faro, V. Marchi, Active U_{11} peptide luminescent gold nanoclusters for pancreatic tumor cell targeting, ACS. Appl. Nano Mater. 6 (10) (2023) 8971–8980, https://doi.org/10.1021/acsanm.3c01594.

[34] R.M. Chiechio, S. Ducarre, G. Moulin, A. Dupont, C. Marets, P. Even-Hernandez, F. Artzner, P. Musumeci, G. Franzò, C. Ravel, M.J. LoFaro, V. Marchi, Luminescent gold nanoclusters interacting with synthetic and biological vesicles, J. Phys. Chem. Lett. 13 (30) (2022) 6935–6943, https://doi.org/10.1021/acs.jpclett.2c01071.

[35] J. Fidy, M. Laberge, A.D. Kaposi, J.M. Vanderkooi, Fluorescence line narrowing applied to the study of proteins, Biochim. Biophys. Acta (BBA) - Protein Struct.

Mol. Enzymol. 1386 (2) (1998) 331–351, https://doi.org/10.1016/S0167-4838(98)00101-0.
[36] K. Pyo, V.D. Thanthirige, K. Kwak, P. Pandurangan, G. Ramakrishna, D. Lee, Ultrabright luminescence from gold nanoclusters: rigidifying the Au(I)–Thiolate shell, J. Am. Chem. Soc. 137 (25) (2015) 8244–8250, https://doi.org/10.1021/jacs.5b04210.
[37] L. Shang, S. Dong, G.U. Nienhaus, Ultra-small fluorescent metal nanoclusters: synthesis and biological applications, Nano Today 6 (4) (2011) 401–418, https://doi.org/10.1016/j.nantod.2011.06.004.
[38] K.L. Wong, J. Liu, Factors and methods to modulate DNA hybridization kinetics, Biotechnol. J. 16 (11) (2021) 2000338, https://doi.org/10.1002/biot.202000338.
[39] P.R. Bueno, Nanoscale Electrochemistry of Molecular contacts. SpringerBriefs in Applied Sciences and Technology, Springer International Publishing: Cham, 2018, https://doi.org/10.1007/978-3-319-90487-0.
[40] B.I. Kurganov, A.V. Lobanov, I.A. Borisov, A.N. Reshetilov, Criterion for Hill equation validity for description of biosensor calibration curves, Anal. Chim. Acta 427 (1) (2001) 11–19, https://doi.org/10.1016/S0003-2670(00)01167-3.
[41] M. Ganau, A. Bosco, A. Palma, S. Corvaglia, P. Parisse, L. Fruk, A.P. Beltrami, D. Cesselli, L. Casalis, G. Scoles, A DNA-based nano-immunoassay for the label-free detection of glial fibrillary acidic protein in multicell lysates, Nanomed.: Nanotechnol. Biol. Med. 11 (2) (2015) 293–300, https://doi.org/10.1016/j.nano.2014.04.006.
[42] F. Chiavaioli, C. Gouveia, P. Jorge, F. Baldini, Towards a uniform metrological assessment of grating-based optical fiber sensors: from refractometers to biosensors, Biosensors 7 (2) (2017) 23, https://doi.org/10.3390/bios7020023.